

Scaling of the $L_{2,3}$ circular magnetic x-ray dichroism of Fe nitrides

M. Alouani

*Department of Physics, The Ohio State University, Columbus Ohio 43210-1368
and IPCMS, Université Louis Pasteur, 13, rue de loess, Strasbourg, France*

J. M. Wills

Los Alamos National Laboratory, Los Alamos, New Mexico 87545

J. W. Wilkins

Department of Physics, The Ohio State University, Columbus Ohio 43210-1368

(Received 18 December 1997)

We have implemented the calculation of the x-ray-absorption cross section for left- and right-circularly polarized x-ray beams within the local-density approximation by means of our all-electron full-relativistic and spin-polarized full-potential linear muffin-tin orbital method. We show that the $L_{2,3}$ circular magnetic x-ray dichroism of Fe, Fe_3N , and Fe_4N compounds scales to a single curve when divided by the local magnetic moment. Sum rules determine the spin and orbital magnetic moment of iron atoms in these ordered iron nitrides. [S0163-1829(98)07315-9]

X-ray-absorption spectroscopy (XAS) can probe selectively each core orbital of each atomic species in a material. Two decades ago the theoretical work of Erskine and Stern showed that the x-ray absorption could be used to determine the circular magnetic x-ray dichroism (CMXD) in transition metals when left- and right-circularly polarized x-ray beams are used.¹ In the last few years these ideas were implemented experimentally, and it became clear that XAS could be used experimentally to determine the local magnetic properties of each magnetic atomic orbital in a magnetic compound.^{2,3} Thus the circular magnetic x-ray dichroism is an important tool for the investigation of magnetic materials,²⁻¹³ especially through the use of sum rules for the direct determination of the local orbital and spin contributions to the total magnetic moment.⁷

The sign of the dichroic signal just above the threshold of absorption allows the determination of the sign of the spin moment of each atom with respect to the total magnetic moment of the system. For example, in the K edge of iron in all rare-earth compounds, the sign of the CMXD yields directly the direction of the magnetic moment on iron atoms.¹⁴ A positive or negative sign of CMXD just above the Fermi level means that the magnetic moment of iron is parallel or antiparallel to the net magnetization. At the rare-earth site, for L_3 absorption a positive or negative CMXD means that the total $4f$ spin is antiparallel or parallel, respectively, to the magnetization (the situation is exactly opposite to that of the L_2 edge). The L_2 (L_3) characteristic is due to the fact that the coupling between $5d$ and $4f$ spins is always ferromagnetic.¹⁵ The direction of the magnetic moment at the rare-earth site is given by the direction of the coupling between L (the orbital component) and S (spin component) according to Hund's rules.

The circular magnetic x-ray dichroism is related to the magnetic moment of the photoexcited atom when the core electron is excited to the conduction states that are responsible for the magnetic properties of the material. For the iron

nitrides we compare the magnetic behavior of iron in these systems to bcc Fe. Experimentally, the spin magnetic moment of Fe varies from $1.5\mu_B$ in hexagonal Fe_3N to $3.0\mu_B$ for the Fe(I) site in cubic Fe_4N .¹⁶

On the theoretical side, Ebert and his co-workers^{8,9} have developed a fully relativistic local-spin-density-approximation approach that was used with success to calculate the CMXD at the K edge of Fe, the L_3 edge of gadolinium, and Fe and Co multilayers. However, their treatment is not self-consistent and uses muffin-tin potentials.^{13,9} Wu, Wang, and Freeman used slab linear augmented plane wave (LAPW) method to study the $L_{2,3}$ CMXD of Fe.¹³ Brouder and co-workers use multiple-scattering theory to solve the Schrödinger equation using spherical potentials and spin-orbit coupling as a perturbation in the final state.¹⁰ Recently Ankudinov and Rehr used a method based on a nonrelativistic treatment of propagation based on high-order multiple-scattering theory and spinor-relativistic Dirac-Fock treatment of the dipole matrix elements to calculate the Fe K edge and Gd L_3 edge CMXD.¹¹

In this paper we study the CMXD at the $L_{2,3}$ edge of iron in iron nitrides, Fe_3N , and Fe_4N . We plan to present our calculation of the K edge elsewhere. We first calculate the CMXD in pure bcc Fe for which most experimental results are available, then we compare our results of Fe nitrides with those of Fe. To our knowledge there is no experimental or theoretical calculation of the $L_{2,3}$ CMXD for any of the Fe nitrides. The analysis of the magnetic states of Fe in Fe-nitride alloys is carried out using the sum rules for the orbital and spin magnetic moment. In particular, we show that (1) sum rules permit the determination of both spin and orbital moments of the different Fe sites in these alloys and (2) the dichroic signal at any Fe site *scales* to a single curve when scaled by its local magnetic moment.

The calculation of the x-ray absorption for left- and right-circularly polarized x-ray beams is implemented within the local-density approximation (LDA) by means of the all-

electron full-relativistic and spin-polarized full-potential linear muffin-tin orbital methods (LMTO).¹⁷ The core electrons are spin polarized and their electronic states are obtained by solving the full Dirac equation, whereas for the valence electrons the spin-orbit coupling is added perturbatively to the semirelativistic Hamiltonian. The total Hamiltonian is then solved self-consistently. To calculate the polarization-dependent cross section we consider the case where the internal field polarizes the spins along the z direction. With respect to this axis we defined the left- and right-circular polarization, which correspond to the photon helicity ($+\hbar$) ($-\hbar$), respectively, and the following dipole interaction: $\hat{\mathbf{e}}_{\pm} \cdot \mathbf{p} = 1/\sqrt{2}(\nabla_x \pm i\nabla_y)$. The absorption cross section μ_{\pm} for left- (+) and right- (-) circular-polarized x ray calculated at the relativistic j_{\pm} ($\ell \pm \frac{1}{2}$) core level and in the dipole approximation is given by

$$\mu_{\pm}(\omega) = \frac{2\pi}{\hbar} \sum_{m_{j_{\pm}}} \sum_{n, \mathbf{k}} \langle j_{\pm} m_{j_{\pm}} | \hat{\mathbf{e}}_{\pm} \cdot \mathbf{p} | n \mathbf{k} \rangle \times \langle n \mathbf{k} | \mathbf{p} \cdot \hat{\mathbf{e}}_{\pm} | j_{\pm} m_{j_{\pm}} \rangle \delta(\omega - E_{n\mathbf{k}} + E_{j_{\pm}}) \quad (1)$$

using LDA in conjunction with the relativistic full-potential LMTO technique.

We have neglected the conduction-electron spin relaxation due to the presence of the core hole. We believe that this relaxation time for ferromagnetic systems with a small spin-orbit coupling is very large compared to the electron-hole recombination. This is because iron is ferromagnetic and the spin relaxation of the conduction states is mainly due to the spin-flip processes. Within local-spin-density approximation (LSDA), when an electron is removed from the core states and added to the conduction electrons, the ground state is such that the electronic configuration of the atom with the core hole is very close to that of the next atom in the periodic table. For Fe plus one electron, LSDA produces a ground state where the electronic configuration of the Fe atom with the core hole is very close to that of Ni.¹⁸ In reality, this spin relaxation produced by spin flip never happens within the lifetime of the photoelectron because Fe has a small spin-orbit coupling constant. The reason LSDA produces the relaxed spin state is because it does not know about relaxation times and the mechanism leading to the final electronic configuration. LSDA just tells us that, given the number of up and down spins at hand, they could be rearranged so that the total energy is minimal. The charge relaxation itself without spin relaxation may be important but cannot be obtained within the present formalism. Thus we believe that, for ferromagnetic materials, the physics of conduction-electron relaxation due to the core hole is beyond the scope of LSDA. However, for paramagnetic materials where there is only charge relaxation, LDA does a nice job in providing the relaxation of $N+1$ electrons due to the core hole.¹⁹

For paramagnetic systems the conduction-state relaxation due to the core hole can be large, and one-electron theory neglecting the conduction-electron relaxation would show discrepancy with experiment. Also we recognize that processes, such as the Coster-Kronig decay, would be partially responsible for the L_3/L_2 branching ratio in absorption and CMXD. The study of such electron-hole interactions requires the calculation of a time-dependent two-electron Green's

function and is beyond the scope of this study. An attempt by Zaanen *et al.*, using an atomic model with some adjustable parameters, demonstrates the influence of the atomic Coulomb and exchange interactions on the L_3 to L_2 branching ratio.²⁰

The spin-polarized core electrons are allowed to relax during the self-consistent calculation. We use the exchange-correlation potential and energy in the von Barth and Hedin approximation.²¹ For the Brillouin zone integration of the density of states and the absorption spectrum we use the tetrahedron method with about 300 \mathbf{k} points in the irreducible part of the Brillouin zone (IBZ).²² Our \mathbf{k} mesh is shifted rigidly by half a step along the x , y , and z axis from the Γ point to avoid using high symmetry points in the IBZ. This shift will avoid the use of degenerate eigenvalues in the BZ integration.

Iron-nitride alloys have been experimentally studied since the 1930's,²³ and their phase diagram is very complex.²⁴ The hexagonal Fe_3N structure (with a double unit formula per unit cell and a $P322$ space group) is very stable over a wide temperature range.²⁴ The cubic Fe_4N structure has iron atoms on the sites of a fcc lattice with a nitrogen at the center of the cube. Its space group is $Fm3m$ with two types of iron atoms. The Fe atom furthest from the nitrogen is denoted Fe(I) ($d_{\text{Fe(I)-N}} = 3.29 \text{ \AA}$) and the closest one Fe(II) ($d_{\text{Fe(II)-N}} = 1.9 \text{ \AA}$). The nitrogen expands the Fe fcc sublattice 10% ($a = 3.797 \text{ \AA}$) with respect to fcc $\gamma\text{-Fe}$. This expansion effect creates a high spin ferromagnetism²⁷ (iron atoms with d^7 configuration resulting in 50% larger moment than $\gamma\text{-Fe}$) as experimentally observed by neutron diffraction.¹⁶

Figure 1 compares our calculated $L_{2,3}$ edge and CMXD for bcc Fe with the experimental results (dashed curve) of Chen *et al.*⁵ We have presented three theoretical curves. In the first curve, called theory 1, a Lorentzian of widths of 0.9 eV and 1.4 eV is used for L_2 and L_3 , respectively, in addition to the 0.4 eV Gaussian broadening as proposed by Ebert and co-workers.⁹ In the second curve, called theory 2, the calculated L_2 and L_3 spectra are broadened both by Lorentzians of width 0.9 eV in addition to the 0.4 eV Gaussian broadening. For theory 3 we used a core-hole lifetime of 0.5 eV and conduction-electron energy-dependent width $\Gamma_v(E - E_F)^2/W^2$, representing electron-electron relaxation not included in the band calculation. Here W is the width of the conduction states and E_F is the Fermi level, and Γ_v is a parameter chosen to be 2 eV and 3 eV for L_3 and L_2 , respectively. The energy-dependent broadening is not sensitive to the choice of Γ_v ; its energy dependence is crucial. As Fig. 1 shows, this energy dependence produces a faster fall off of the L_2 and L_3 tails independent of the value of Γ_v . This increases the L_3/L_2 branching ratio and washes out the shoulder at 15 eV in the $L_{2,3}$ spectrum in agreement with experiment. We believe that the energy dependence of the broadening plays a significant role in determining the L_3/L_2 branching ratio for $3d$ transition metals. All the experimental features are reproduced by our calculation. Interestingly, Ebert and co-workers⁹ using spin-polarized relativistic LMTO in its atomic-sphere-approximation implementation produced $L_{2,3}$ spectra which are in good agreement with our full-potential calculation.

Figure 2 shows our calculated Fe $L_{2,3}$ absorption edge at the Fe site for bcc Fe, hexagonal Fe_3N , and cubic Fe_4N for

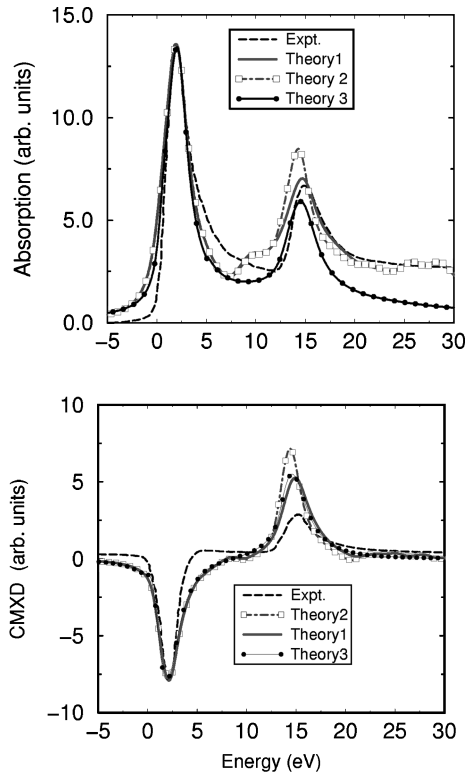


FIG. 1. Calculated x-ray $L_{2,3}$ absorption and circular magnetic dichroism of ferromagnetic Fe compared to the experimental results of Chen *et al.* (dashed curve). For the curve called theory 2 we have broadened our all-electron calculated L_2 and L_3 spectra by Lorentzians of width 0.9 eV and by a Gaussian (full width at half maximum of 0.4 eV). For theory 1 we used a Lorentzian width of 0.9 eV (L_3) and 1.4 eV (L_2) in addition to the 0.4 eV Gaussian broadening as used by Guo *et al.* (Ref. 9). For theory 3 we used a core-hole lifetime of 0.5 eV and energy-dependent width $\Gamma_v(E - E_F)^2/W^2$ representing electron-electron relaxation not included in the band calculation. Here W is the width of the valence states and E_F is the Fermi level, and Γ_v is a parameter chosen to be 2 eV and 3 eV for L_3 and L_2 , respectively.

left- and right-circularly polarized x ray. Note the close similarities of these spectra. The L_2 and L_3 peaks are separated by the $2p_{1/2}$ - $2p_{3/2}$ 12.4 eV spin-orbit splitting compared to the experimental value of 13.0 eV.

Peak ratio. The ratio of L_3 CMXD peak to the L_2 peak is about -1.1 , which is in agreement with the tight-binding band theory ratio of -1 obtained for a realistic value of the spin-orbit coupling parameter,¹² but in disagreement with the experimental ratio of -2.6 .¹² We believe that the strong deviation of the experimental L_2 and L_3 peak intensity ratio from unity is chiefly due to broadening effects, including the energy-dependent electron-electron relaxation and Coster-Kronig decay processes. In bcc Fe the observed width at half maximum of the L_2 white line is almost twice as large as that of the L_3 spectrum (see Ref. 5).

Using a broadening for L_2 1.5 that of the L_3 edge brings the calculated ratio closer to experiment (see Fig. 1). The use of the different broadening effects was also suggested by Ebert and co-workers.⁹ However, the broadening effect will not change the integrated L_2 and L_3 dichroic signals.

Integrated signals and use of the sum rules. Figure 3 shows the $L_{2,3}$ CMXD of Fe_3N in cubic (AuCu_3 structure)

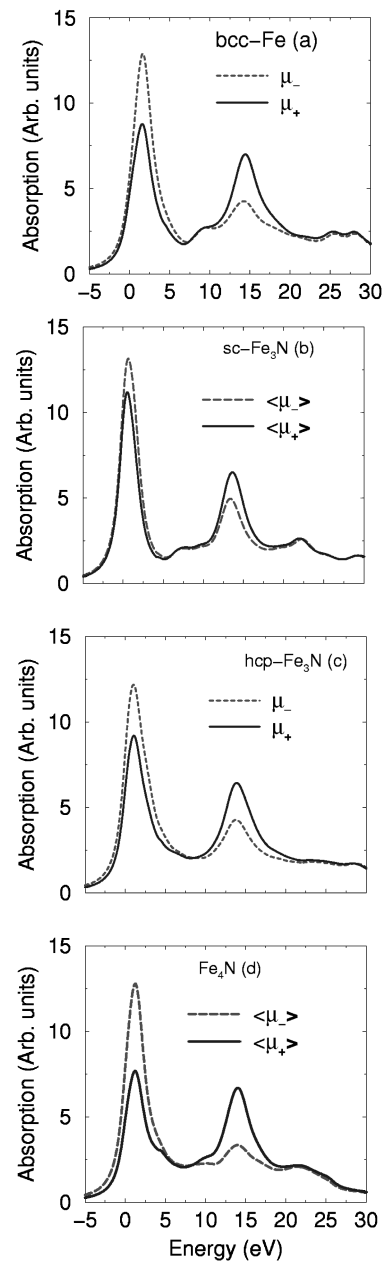


FIG. 2. Left- (dashed curve) and right- (continuous curve) circular-polarized x-ray $L_{2,3}$ absorption spectra for (a) Fe, (b) simple cubic Fe_3N (theory), (c) hexagonal Fe_3N (theory), and (d) Fe_4N (theory). We have used a Lorentzian lifetime broadening of 0.9 and 1.4 eV for L_3 and L_2 , respectively, in addition to the 0.4 eV Gaussian broadening as proposed by Ebert and co-workers.⁹ The spin-orbit coupling between the L_2 and L_3 white line peaks is 12.4 eV compared to the experimental value of 13.0 eV. The Fermi level is at the zero of energy.

and hexagonal structure, cubic Fe_4N and bcc Fe CMXD. Each spectrum is scaled by the local magnetic moment of the selected Fe site. That the scaled spectra fall on a single curve indicates that for these compounds the amplitude and the shape of the CMXD signal are proportional to the local spin magnetic moment.

This scaling is obtained by calculating the local orbital and spin moments using the CMXD sum rules derived using an ion model by Thole and co-workers.⁷ For the $L_{2,3}$ edges these sum rules are as follows:

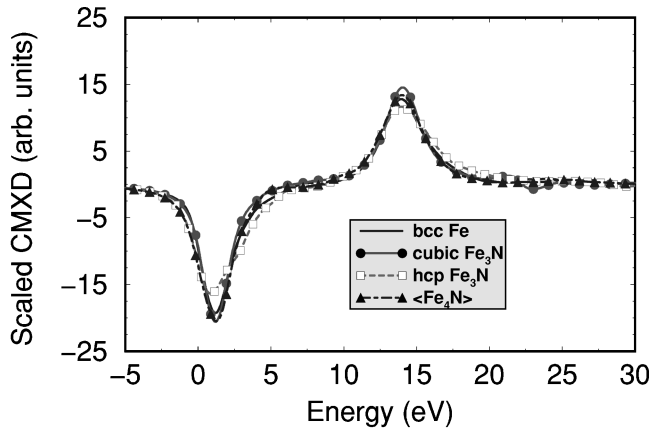


FIG. 3. Calculated circular magnetic dichroism of the $L_{2,3}$ edge at the site of Fe, for ferromagnetic Fe, cubic Fe_3N , hexagonal (hcp), and cubic Fe_3N , and Fe_4N scaled by the spin magnetic moment. All the dichroic curves form a single curve. The Fermi level is at zero of energy.

$$\frac{\int_{L_2+L_3} d\omega[\mu_+(\omega) - \mu_-(\omega)]}{\int_{L_2+L_3} d\omega[\mu_+(\omega) + \mu_-(\omega) + \mu_0(\omega)]} = \frac{\langle L_z \rangle}{2N_h}, \quad (2)$$

$$\frac{\int_{L_3} d\omega[\mu_+(\omega) - \mu_-(\omega)] - 2 \int_{L_2} d\omega[\mu_+(\omega) - \mu_-(\omega)]}{\int_{L_2+L_2} d\omega[\mu_+(\omega) + \mu_-(\omega) + \mu_0(\omega)]} = \frac{\langle S_z \rangle + 7\langle T_z \rangle}{3N_h}. \quad (3)$$

Here $\langle L_z \rangle$ is the expectation value of the orbital moment, $\langle S_z \rangle$ is that of the spin moment, and $\langle T_z \rangle$ that of the magnetic dipole moment, and N_h is the number of holes in the $3d$ orbitals. In cubic materials the $\langle T_z \rangle$ term is induced by only spin-orbit coupling in the conduction states⁹ and is therefore negligible for Fe and cubic Fe nitrides.

To derive these sum rules for solids several approximations were made.⁷ The most severe among these is the ne-

glect of the energy dependence of the radial matrix elements, which is equivalent to ignoring the interatomic hybridization. These approximations will probably limit the validity and usefulness of these sum rules, and a case by case study should therefore be carried out, as has been done for Fe, Co, and Ni.^{9,13}

These sum rules could also be used *experimentally* to deduce the spin and orbital magnetic moments of each magnetic orbital from the CMXD signals, the upper limit of the integral is fixed by the number of holes N_h which is not known, and the subtraction of the background is problematic. However, recently Chen *et al.*⁵ have developed a scheme for directly extracting the orbital and spin moments from the dichroic signals, and deduced the spin and orbital moments of Fe, and Co metals using their experimental CMXD signals. To define the upper limit of the integral of their spectra they introduced an *ad hoc* two-step-like function. We can use our calculation to determine the energy cutoff of the sum-rule integrals by integrating the d density of states to obtain the number of holes in the $3d$ orbitals, finding 4 eV for Fe and its nitrides.²⁸ The sum rules are insensitive to this cutoff; a 2 eV increase changes the magnetic moment by only a few percent.

Table I displays the orbital and the spin magnetic moments as obtained using the sum rules given by Eqs. (2) and (3) using 4.0 eV cutoff above the Fermi level and they are compared to direct calculation and available experimental data. We have found that the spin magnetic moments obtained from these sum rules agree nicely with the spin moment calculated directly from the density of states and experiment, whereas the orbital moment is about 20% smaller than the direct calculation and much smaller than experiment. In the case of bcc Fe, our results are in good agreement with the results of Guo *et al.* using LMTO in its atomic-sphere approximation and Wu, Wang, and Freeman using a slab LAPW.¹³

The underestimation of the experimental orbital moment is likely due to our neglect of the orbital-polarization term in the relativistic Hamiltonian. An inclusion of this term n by Eriksson *et al.*²⁹ appears to remove this discrepancy. However, it is surprising that the orbital moment of Fe in Fe_4N , as produced using the orbital sum rule, is about twice that of pure bcc Fe despite only 50% increase in the spin magnetic

TABLE I. Calculated spin and orbital magnetic moments, in units of μ_B , from the orbital and spin sum rules and from the direct calculation for Fe, Fe_3N , and Fe_4N compounds. The spin and orbital magnetic moments derived from the sum rules, see Eqs. (2) and (3), are denoted by $2\langle S_z \rangle$ and $\langle L_z \rangle$, respectively; the direct calculations are denoted by m_{spin} and m_{orb} , respectively. The experimental results obtained from the sum rules are included between parentheses.

Compounds	$\langle L_z \rangle$	$2\langle S_z \rangle$	m_{orb}	m_{spin}	Expt.
Fe	0.03 (0.086 ^a)	2.16 (1.98 ^a)	0.046	2.16	2.08 ^b
Fe_3N (cubic)	0.02	$\langle 1.20 \rangle$	0.031	$\langle 1.7 \rangle$	
Fe_3N (hex)	0.05	$\langle 1.85 \rangle$	0.040	$\langle 1.97 \rangle$	1.5 ^c
Fe_4N	Fe(I)	0.07	2.96	9.14/ Fe_4N	3.0 ^d
	Fe(II)	0.07	2.34	0.053	2.0 ^d

^aReference 5.

^bReference 26.

^cReference 25.

^dReference 16.

moment. We attribute this sharp increase to the difficulty of obtaining the orbital moment from the sum rule given by Eq. (2) which subtracts two small numbers. The direct calculation produced, however, an increase comparable to that of the spin magnetic moment.

In conclusion, we have calculated the circular magnetic x-ray dichroism within our all-electron local-density approximation in conjunction with the full-potential linear muffin-tin orbital method. The spin-orbit coupling is found to be crucial for the calculation of the CMXD signal. We have determined the $L_{2,3}$ edges of Fe, and the $L_{2,3}$ edges of Fe_3N and Fe_4N nitrides. The most important result is that the intensity of the dichroic signal is proportional to the spin magnetic moment at the iron site, i.e., when the CMXD curves are scaled by the local magnetic moment they all fall in a single curve.

The recently derived sum rules for the orbital and spin magnetic moments are tested for these compounds and the spin magnetic moment obtained from these sum rules agrees with the direct calculation and with the experimental results whereas the orbital moment is somewhat underestimated. We have attributed this discrepancy to our neglect of the orbital-polarization term in the LDA Hamiltonian.²⁹

One of us (M.A.) thanks Ch. Brouder, E. Dartyge, H. Ebert, C. Giorgetti, and J. Rehr for useful discussions. This research was supported in part by the U.S. Department of Energy, Basic Energy Sciences, Division of Materials Sciences, and by NSF, Grant No. DMR-9520319. Supercomputer time was provided by the Ohio State Supercomputer Center.

-
- ¹J. L. Erskine and E. A. Stern, Phys. Rev. B **12**, 5016 (1975).
²G. van der Laan *et al.*, Phys. Rev. B **34**, 6529 (1986).
³G. Schütz *et al.*, Phys. Rev. Lett. **58**, 737 (1987).
⁴P. Carra and M. Alterelli, Phys. Rev. Lett. **64**, 1286 (1990).
⁵C. T. Chen *et al.*, Phys. Rev. Lett. **75**, 152 (1995), and references therein.
⁶P. Carra *et al.*, Phys. Rev. Lett. **66**, 2495 (1991).
⁷For atoms: B. T. Thole *et al.*, Phys. Rev. Lett. **68**, 1943 (1992); P. Carra *et al.*, *ibid.* **70**, 694 (1993); for solids: A. Ankudinov and J. J. Rehr, Phys. Rev. B **51**, 1282 (1995).
⁸H. Ebert, P. Strange, and B. L. Gyorffy, J. Appl. Phys. **63**, 3055 (1988).
⁹G. Y. Guo *et al.*, Phys. Rev. B **50**, 3861 (1994); E. Ebert, Rep. Prog. Phys. **59**, 1665 (1996).
¹⁰Ch. Brouder, M. Alouani, and K. H. Bennemann, Phys. Rev. B **54**, 7334 (1996), and references therein.
¹¹A. Ankudinov and J. J. Rehr, Phys. Rev. B **56**, 1712 (1997).
¹²N. V. Smith, C. T. Chen, F. Sette, and L. F. Mattheiss, Phys. Rev. B **46**, 1023 (1992).
¹³R. Wu, D. Wang, and A. J. Freeman, Phys. Rev. Lett. **71**, 3581 (1993); R. Wu and A. J. Freeman, *ibid.* **73**, 1994 (1994).
¹⁴C. Giorgetti, Ph.D. thesis, Université Sud, Orsay, 1992.
¹⁵I. A. Campbell, J. Phys. F **2**, L47 (1977).
¹⁶B. C. Frazer, Phys. Rev. **12**, 751 (1958).
¹⁷J. M. Wills (unpublished). For a general review of LMTO see O. K. Andersen, Phys. Rev. B **12**, 3060 (1975).
¹⁸M. Alouani, Phys. Rev. B **49**, 16 038 (1994).
¹⁹For a review see U. von Barth and G. Grossman, Phys. Rev. B **25**, 5150 (1982); Phys. Scr. **26**, 107 (1983); M. Alouani, J. M. Koch, and M. A. Khan, Solid State Commun. **60**, 657 (1986).
²⁰J. Zaanen *et al.*, Phys. Rev. B **32**, 4905 (1985).
²¹U. von Barth and L. Hedin, J. Phys. C **5**, 1629 (1972).
²²O. Jepsen and O. K. Andersen, Solid State Commun. **9**, 1763 (1971); G. Lehmann and M. Taut, Phys. Status Solidi B **54**, 469 (1972).
²³B. Hendricks and R. Kesting, Z. Kristallogr. **74**, 511 (1930).
²⁴K. H. Jack, Acta Crystallogr. **5**, 404 (1952).
²⁵M. Robbins and J. G. White, J. Phys. Chem. Solids **25**, 717 (1964).
²⁶K. Adachi *et al.*, in *Magnetic Properties of Metals*, edited by H. P. J. Wijn, Vol. 19 of *Landolt-Börnstein: Numerical Data and Functional Relationships in Science and Technology*, New Series, Group III, Pt. a, edited by K.-H. Hellwege and O. Madelung (Springer-Verlag, Berlin, 1986), p. 178.
²⁷V. L. Moruzzi *et al.*, Phys. Rev. B **34**, 1784 (1986).
²⁸The tail of the d states due to hybridization extends to higher energies, making the cutoff energy higher than the canonical d density-of-states maximum. We have used the maximum of the canonical d density of states which is about 4 eV above the Fermi level.
²⁹O. Eriksson *et al.*, Phys. Rev. B **45**, 2868 (1992); **41**, 11 807 (1990).